Random telegraph signal (RTS) in the Euclid IR H2RGs

Ralf Kohley, Luca Conversi, Pierre-Elie Crouzet, Paolo Strada, Rémi Barbier, Sylvain Ferriol, Bogna Kubik, Aurélia Secroun, Jean-Claude Clémens, Anne Ealet, et al.

Random telegraph signal (RTS) in the Euclid IR H2RGs

Ralf Kohley*[a], Rémi Barbier[b], Jean-Claude Clémens[c], Luca Conversi[a], Pierre-Elie Crouzet[d], Anne Ealet[c], Sylvain Ferriol[b], William Gillard[c], Bogna Kubik[b], Cyrille Rosset[e], Aurélia Secroun[c], Benoît Serra[c,f], Paolo Strada[d]

[a]European Space Agency / ESAC, Camino Bajo del Castillo, 28692 Villanueva de la Cañada, Spain;
[b]Institut de Physique Nucléaire de Lyon (IPNL), 4, Rue Enrico Fermi, 69622 Villeurbanne, France;
[c]Centre de Physique des Particules de Marseille (CPPM), 163, Avenue de Luminy, 13288 Marseille, France;
[d]European Space Agency / ESTEC, Keplerlaan 1, 2201 AZ Noordwijk, The Netherlands
[e]Laboratoire Astroparticule et Cosmologie (APC), 10, rue Alice Domon et Léonie Duquet, 75013 Paris, France;
[f]European Southern Observatory, Karl-Schwarzschild-Str. 2, 85748 Garching, Germany

ABSTRACT

Euclid is an ESA mission to map the geometry of the dark Universe with a planned launch date in 2021. Euclid is optimised for two primary cosmological probes, weak gravitational lensing and baryonic acoustic oscillations. They are implemented through two science instruments on-board Euclid, a visible imager (VIS) and a near-infrared photometer/spectrometer (NISP), which are being developed and built by the Euclid Consortium instrument development teams. The NISP instrument contains a large focal plane assembly of 16 Teledyne HgCdTe H2RG detectors with 2.3 µm cut-off wavelength and SIDECAR readout electronics. The performance of the detector systems is critical for the science return of the mission and extended on-ground tests are being performed for characterisation and calibration purposes. Special attention is given also to effects even on the scale of individual pixels, which are difficult to model and calibrate, and to identify any possible impact on science performance. This paper discusses the known effect of random telegraph signal (RTS) in a follow-on study of test results from the Euclid NISP detector system demonstrator model [1], addressing open issues and focusing on an in-depth analysis of the RTS behaviour over the pixel population on the studied Euclid H2RGs.

Keywords: Euclid, RTS, RTN, H2RG, HgCdTe, NISP

1. INTRODUCTION

The combined focal plane for the Near-Infrared Spectrometer and Photometer (NISP) of the ESA medium class mission Euclid (see [2] and [3] for further details on the Euclid mission and NISP) consists of 16 individual detector systems called Sensor Chip Systems (SCS) arranged in an array of 4 by 4 SCS in the focal plane assembly (FPA). The SCS comprises a HgCdTe H2RG detector with 2.3µm cut-off wavelength called the Sensor Chip Assembly (SCA), a cryogenic flex cable (CFC) and the SIDECAR readout electronics called Sensor Chip Electronics (SCE). This triplet of SCA, CFC and SCE are custom made by Teledyne Imaging Sensors (TIS) for the Euclid mission and provided by NASA through JPL with characterisation and acceptance testing under responsibility of the Detector Characterization Laboratory (DCL) at Goddard Space Flight Center (GSFC). More details on the Euclid SCAs can be found in [4].

After delivery to the NISP team the flight detector systems undergo an extensive calibration campaign at the Centre de Physique des Particules de Marseille (CPPM) before assembly into the NISP focal plane and continuing tests at instrument level at the facilities of the Laboratoire d'Astrophysique de Marseille (LAM). The calibration campaign at CPPM (Flight Model (FM) calibration campaign) was scheduled in blocks of 4 SCS tested in parallel in two identical cryostats, each test block lasting more than 1.5 months to complete, and coming now to its end with the final testing of the 4 Flight Spare SCAs. The description of the overall test campaign as well as the overall calibration strategy are presented in two additional Euclid papers of this conference (see [5] and [6]).

*ralf.kohley@esa.int

For the follow-up study of the effect of random telegraph signal (RTS) and noise (RTN) in the Euclid infrared H2RGs, we analysed data from all 16 Flight SCAs tested at CPPM together with data from additional tests on two non-flight SCAs at ESA's European Space Research and Technology Centre (ESTEC) and at CPPM. These test campaigns were primarily dedicated to the investigation of radiation effects in one case and the photometric and centroiding impact of crosshatch patterns in the other case (see [7] for more details).

2. RANDOM TELEGRAPH SIGNAL AND NOISE

For the original study of RTS on the Euclid IR H2RGs an algorithm was developed and validated for detection of two-state RTS using long sampling up-the-ramp (UTR) dark acquisitions during the Euclid demonstrator model tests. A summary of the algorithm, analysis and the lessons-learnt from this study are presented below and can be found in detail in [1] and references therein.

Compared to the dark current RTS, which is not the subject of this paper and a property of the charge generation mechanisms within the HgCdTe infrared diode, the analysed RTS here is the spontaneous change of the pixel reset value (also called pedestal or baseline) between two defined states and believed to be caused by trapping / de-trapping in the per-pixel source follower structure of the H2RG CMOS circuits. Figure 1 from [1] shows an example of two distinct RTS flavours, one (left) of high frequency short release time trapping, and another one (right) of low frequency long release time trapping. Both types appear in the Euclid H2RG, while the high frequency, "spike-like" type predominates. The RTS phenomenon is classified through three parameters as shown in Figure 1: amplitude, period and time in high state. Period and time in high state are not fully independent with periods approaching 2 frames (e.g. highest frequency) the time in high state necessarily goes to 50%.

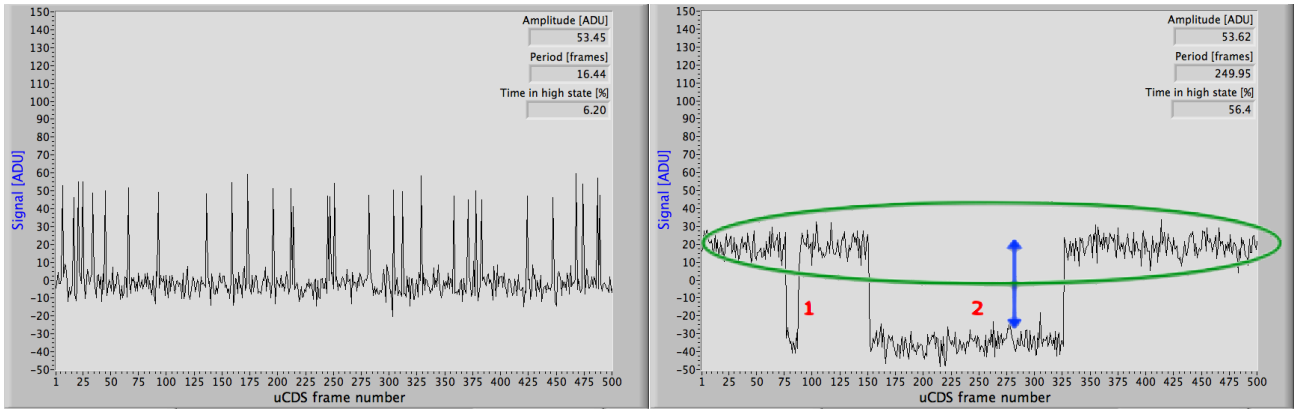

Figure 1: Two examples of RTS noise flavours. The plots show the apparent signal measured in the two pixels after reset with the reset signal subtracted (e.g. Correlated Double Sampling or CDS) over a sampling up-the-ramp (UTR) acquisition of 500 frames. For clarity the signal slopes corresponding to the dark signal ramps have been subtracted as well. (Left) High frequency, spike-like baseline excursions. (Right) Low frequency square-wave transitions with nearly equal time in high and low states. The characteristics leading to the three RTS parameters are marked on the plot to the right: amplitude (blue double arrow), number of transition pairs (2 in red, leading to period of 250 over 500 frames) and the frames related to time in high state (encircled in green).

The assumed origin of this read-out RTS in the CMOS circuit is supported by the fact that proportionally as many RTS pixels were found in the population of reference pixels as in the image area, both at around 1% of all pixels limited by the detection algorithm efficency. It was further found that 95% of all detected RTS pixels had amplitudes below 300e- with a skewed distribution towards the detection threshold. In essence the RTS during UTR acquisitions presents a non-white noise component, termed random telegraph noise (RTN).

The algorithm is taking the Correlated Double Sampling (CDS) time series (see Figure 1 and caption for explanation) of long (about 2h) UTR over 5000 frames (frame time about 1.45s) and trying to fit 2 Gaussian distributions to a histogram of the CDS frame signal values. If the fit fails, the pixel is not considered a RTS candidate. Otherwise the three RTS parameters are extracted as shown in Figure 2 taken from [1].

Using simulations the algorithm has shown very high detection efficiency on the long UTR acquisitions of 95% and no false positives from noisy pixels, if the amplitude threshold is set at least 3-sigma readout noise. Other algorithms were considered for the follow-up study, but due to the excellent results, the original algorithm was maintained unaltered.

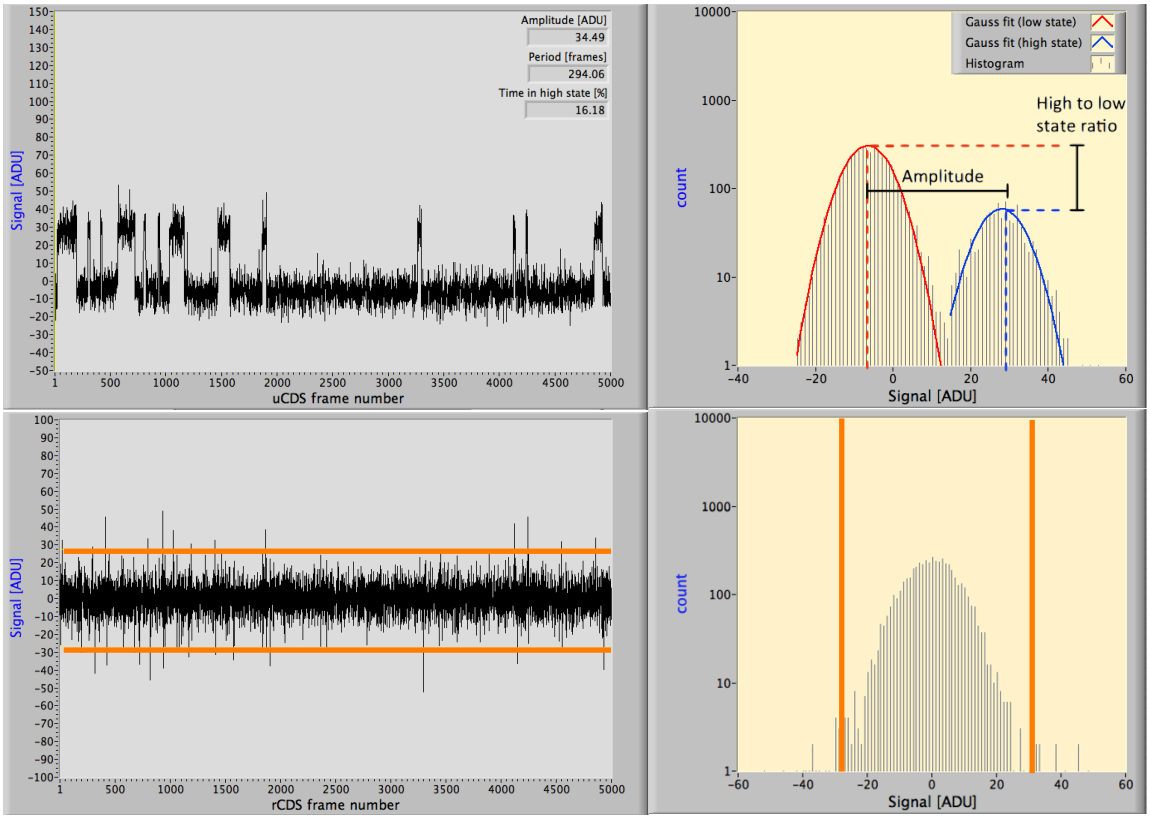

Figure 2: Example of RTS noise pixel analysis: (Upper left) Timeline of UTR CDS signal values. The analysis results are given as well. (Upper right) Histogram of the UTR CDS signal values. Two Gaussian envelopes have been fitted to the distributions belonging to the low and high states. The difference in Gaussian peak positions gives the estimate for the RTS noise amplitude. The peak heights are taken as measure for the time in high to low state ratio assuming similar distribution widths. (Lower left) The corresponding "rate" CDS values (differentiation of the upper left plot) and the estimated thresholds to count the number of positive and negative transition. These give an estimation of the RTS period. (Lower right) The histogram of the rate CDS values. The few and not spike-like transitions appear as outliers and not as separate populations like in the case of high frequency RTS.

Glitches from cosmic rays, high dark current and instable pixels (drifting baseline, etc.) need to be filtered out separately though. Cosmic ray impacts were filtered out by only considering common RTS candidates from multiple ramps or limiting the highest period (single transitions) and high dark current by setting a threshold on the maximum flux. To increase the detection efficiency to 100% and to filter instable pixels, the minimum amplitude can be set far above the 3-sigma noise threshold. These "stable" reduced RTS populations can then be used also to individually inspect each RTS pixel visually.

3. RTS DEPENDENCIES

In the original study RTS was found to have dependencies, most of which needed further in-depth study. Dedicated analyses were therefore carried out to address them separately.

3.1 Thermal Cycles

The influence of thermal cycles on the RTS population has been investigated on two dark UTR ramps on the same Flight SCA but matched to a different SCE and therefore subject to a thermal cycle in between. The first data set was taken in

April 2017 and the second one in September 2017, therefore also time and annealing at room temperature could play a role.

To avoid any problems with noisy pixels contaminating the RTS statistics, only detected RTS with minimum amplitude of 50e- were considered, e.g. a "stable" subset of RTS pixels. The number statistics is presented in Table 1. As can be seen from the table there is quite some variability and only about 60% of detected RTS pixels were still present after the thermal cycle (common RTS pixels). Roughly the same amount of RTS pixels were appearing new ("new" RTS pixels) as those that had disappeared ("lost" RTS pixels). Reasons for this variability are several and are listed below, not all related to any actual impact of thermal cycling, but to the algorithm performance:

- True disappearance / appearance of RTS on pixels
- Changes in RTS morphology (amplitude, frequency, time in high state)
- Limited precision in amplitude determination (jitter around amplitude threshold for RTS selection)
- Glitches (cosmic ray impacts) on RTS pixels
- Non-linear background flux (persistence effects, for example) leading to distorted histograms
- Low frequency RTS not presenting transitions during 2h UTR (or single transitions and filtered out as glitches)

A quantification of these possible contributors to the derived overall number statistics is still outstanding. To indeed confirm that RTS appears and disappears visual inspection of the CDS time lines on several RTS pixels has been carried out and some examples are presented in Figure 3 and Figure 4. Changes in the morphology of the CDS time lines, e.g. changes to the RTS parameters, have been found as well and examples are shown in Figure 5.

For the common RTS pixels, e.g. those detected before and after thermal cycle, correlation plots for the three RTS parameters have been made, shown in Figure 6. The plots reveal that in the frame of the algorithm precision to retrieve these parameters, the RTS population characteristics remained largely unchanged.

Long UTR ramps in darkness taken at ESTEC for the thermal cycle investigation on an engineering grade SCA unfortunately showed some noise pick-up, which rendered the RTS analysis unstable and could finally not be used. These dedicated tests over the course of a few days will be repeated in due time.

Interpretation of the results is therefore still to be taken with caution pending disentangling any time and/or annealing effects from the true thermal cycle impact and quantification of contributors to the number statistics variability.

Table 1: RTS number counts before and after thermal cycle

Data set	Date	Operating temperature	Detected RTS (image area), amplitude ≥ 50e-
Before thermal cycle	April 2017	80 K	4787
After thermal cycle	September 2017	80 K	5279
Common RTS pixels			3140
"Lost" RTS pixels			1647
"New" RTS pixels			2139

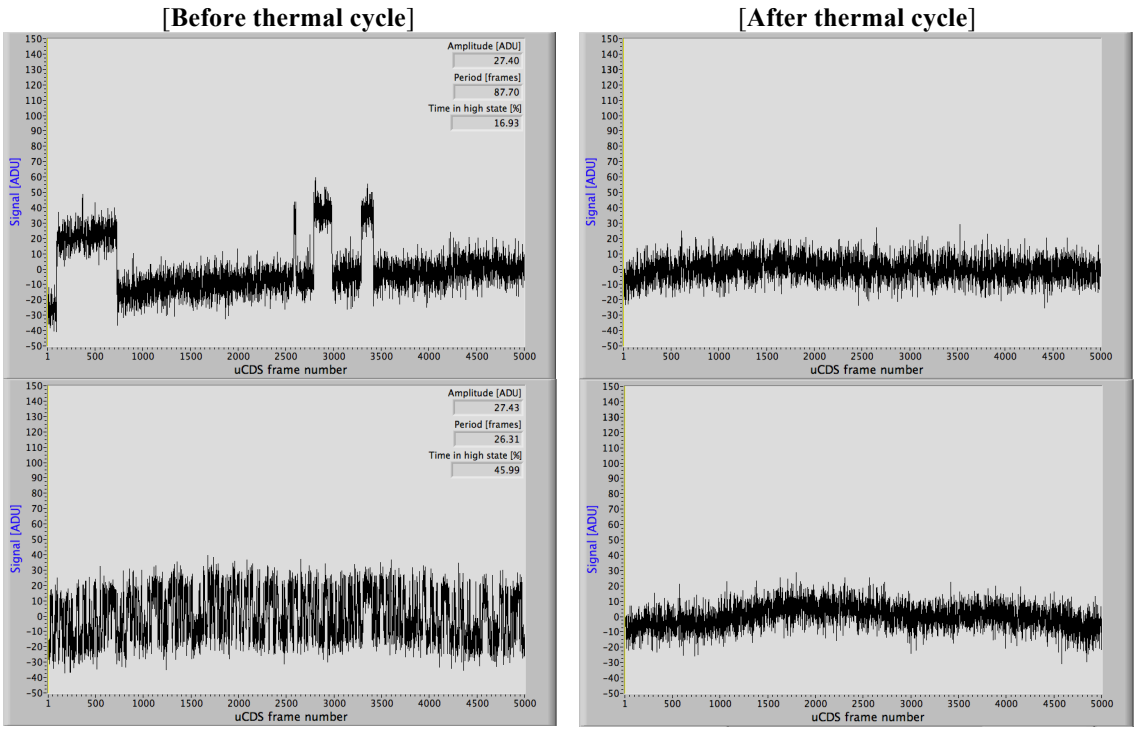

Figure 3: Examples of "disappearance" of RTS on pixels before and after thermal cycling (lost RTS pixels). Linear dark current contribution has been subtracted from the shown CDS time lines.

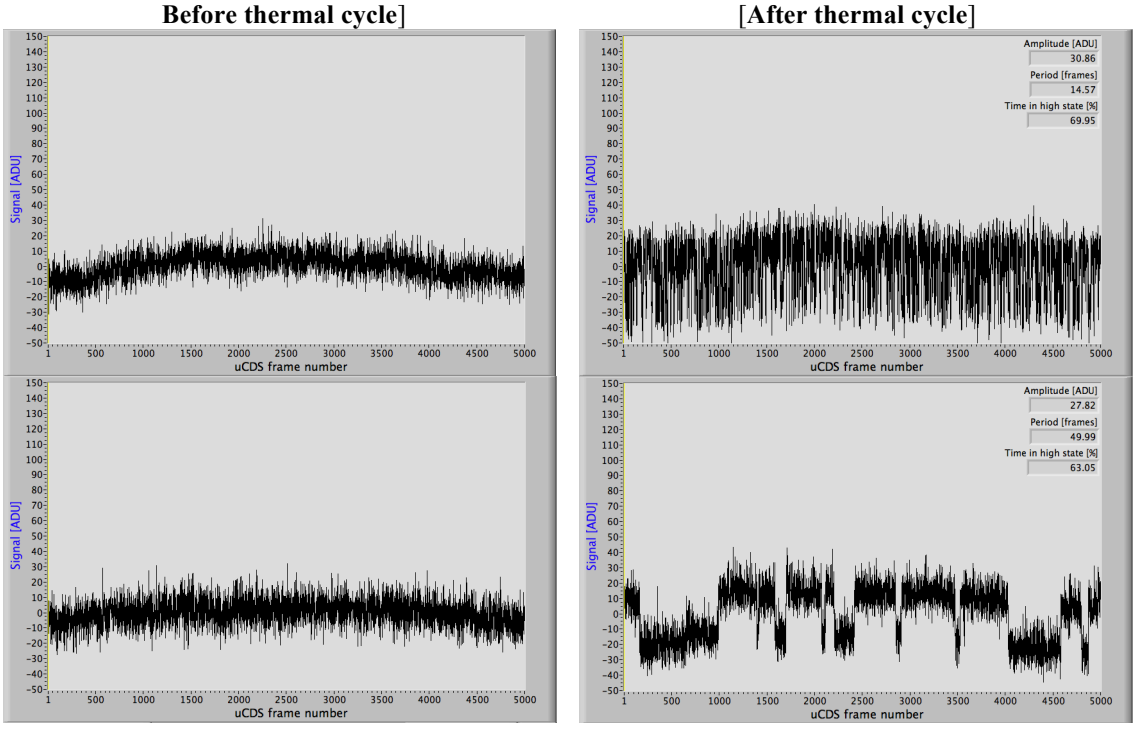

Figure 4: Examples of "appearance" of RTS on pixels before and after thermal cycling. Linear dark current contribution has been subtracted from the shown CDS time lines.

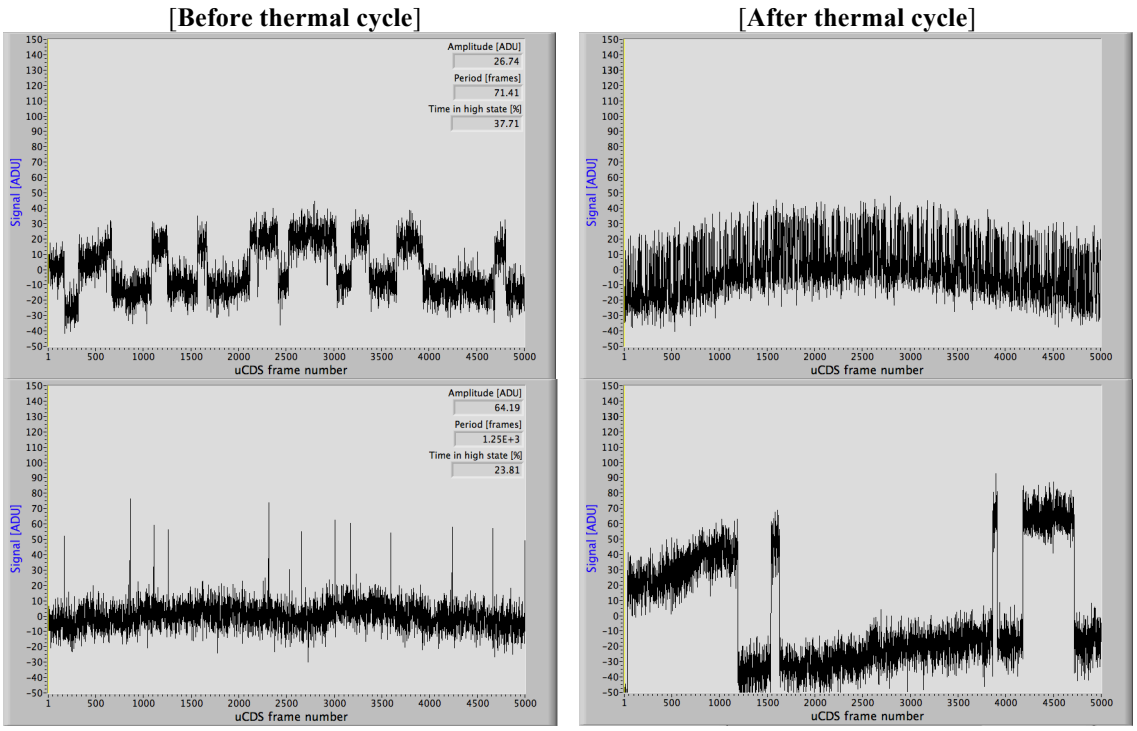

Figure 5: Examples of RTS morphology changes before and after thermal cycling. All parameters (amplitude, frequency and time in high state) can be affected. Linear dark current contribution has been subtracted from the shown CDS time lines.

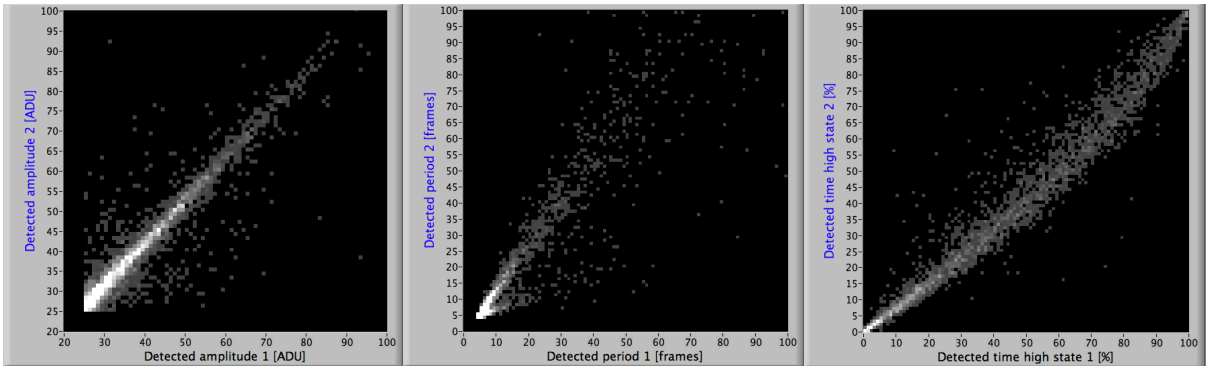

Figure 6: Correlation plots for the 3 RTS parameters on the 60% common RTS detected before thermal cycle (UTR "1") and after (UTR "2"); (Left) amplitude, (Middle) period, (Right) time in high state. Considering the precision of parameter value retrieval of the used algorithm, it can be considered that the parameters stay stable, e.g. the RTS type stays unaltered.

3.2 Radiation

Proton beam cold irradiations were carried out in December 2016 at the UCL Cyclotron Resource Centre in Louvain-la-Neuve (Belgium) with a proton fluence of $3.75 \cdot 10^{11}$ p/cm^2 (~39 MeV proton energy, downgrade from 65 MeV beam energy) projected on a circular area in the centre of the SCA. The irradiation fluence was administered in two fluxes, a low flux during which the detector system acquired images in order to record the proton-induced glitches and a high flux with the SCA switched off. While the irradiation was with the SCA at cryogenic temperature (90K) and frames were acquired during the low flux irradiation, the sequences were not appropriate for the RTS study. The same SCA had been

characterized though before the irradiation during a pilot run of the FM calibration campaign at CPPM in August 2016 and then again after the irradiation in January 2017. Unfortunately the detector could not have been kept cold, so room temperature annealing for a few weeks is assumed together with two thermal cycles. Only permanent or slowly annealing radiation damage could be detected this way, also considering the caveats reported in section 3.1 due to thermal cycling and long ambient temperature storage.

Due to the location and size of the proton irradiation beam (see Figure 7) only the central part of the detector was irradiated leaving the other edges of the image area and the reference pixels (4 pixel wide outer frame around the image area not connected to the infrared diode and used for common-mode noise reduction) as quasi non-irradiated control regions. Any irradiation-induced effect should therefore show similarity in geometrical distribution to the irradiation footprint.

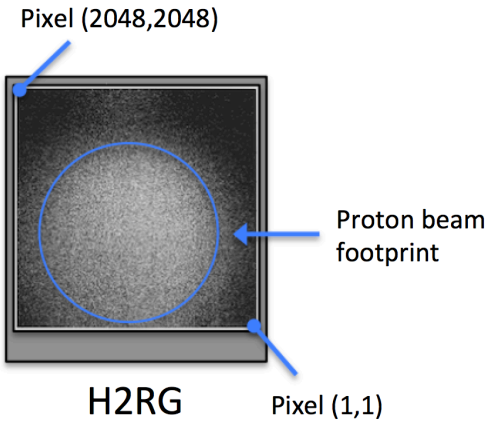

Figure 7: Schematic of the proton irradiation beam footprint on Euclid H2RG image area. The image shows the proton-induced glitches recorded in UTR acquisitions during low flux irradiation.

Unfortunately, the reference pixels on the dark ramps taken after irradiation were presumably subject to some noise pick-up, which let to false detections of "new" RTS pixels of spike-like, high frequency morphology with roughly the same amplitude, mostly aligned to the outer rim of reference pixels. The histograms before and after irradiation are shown below in Figure 8. This effect nevertheless is still under investigation.

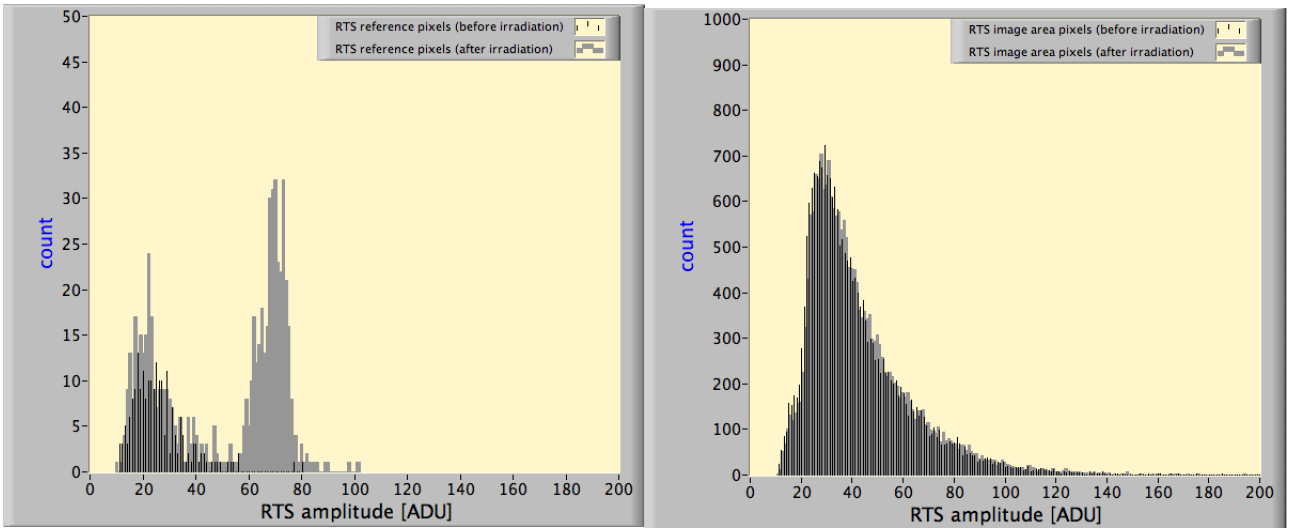

Figure 8: Histograms of amplitudes of detected RTS before irradiation (thin bars) and after irradiation (thick bars). There is some variation in number counts for the reference pixels population (left histogram) showing a strong new population peaking around 65 ADU, but caused by noise pick-up and therefore false RTS detection. The image area pixels (right histogram) essentially show no increase in RTS population or any modification of RTS properties.

In the further analysis therefore only image area pixels were considered. Apart from reporting all RTS candidates also an amplitude threshold of 35e- was set to obtain a more stable and less noisy-pixel contaminated subset. The low threshold has been set to allow identifying enough RTS pixels for the density plots in order to have statistics for any geometrical correlation analysis. The numbers are presented in Table 2 and the density plots of all disappeared RTS pixels and all newly appeared RTS pixels are shown in Figure 9. The detected new RTS pixels are rather randomly distributed and show no geometrical similarity to the irradiation pattern.

Furthermore, as for the thermal cycle analysis, the table shows much variability and only about 75% of all RTS pixels were also detected after irradiation. Again, roughly the same amount of RTS pixels were appearing new ("new" RTS pixels) as those that had disappeared ("lost" RTS pixels). Most of the variability might be attributed to the reasons given in section 3.1 (thermal cycles). As for the thermal cycle analysis the correlation plots have been derived for the three RTS parameters of the common RTS pixels and no measurable effect has been detected. Considering additionally any missing geometrical likelihood of RTS distribution to the irradiation pattern, it is very likely that irradiation has no impact on the RTS population.

Table 2: RTS number counts before and after irradiation

Data set	**Date**	**Operating temperature**	**Detected RTS (image area), all RTS candidates**	**Detected RTS (image area), amplitude ≥ 35e-**
Before irradiation	August 2016	90 K	21544	17070
After irradiation	January 2017	90 K	21229	17613
Common RTS			16117	13513
"lost" RTS			5427	3557
"new" RTS			5112	4100

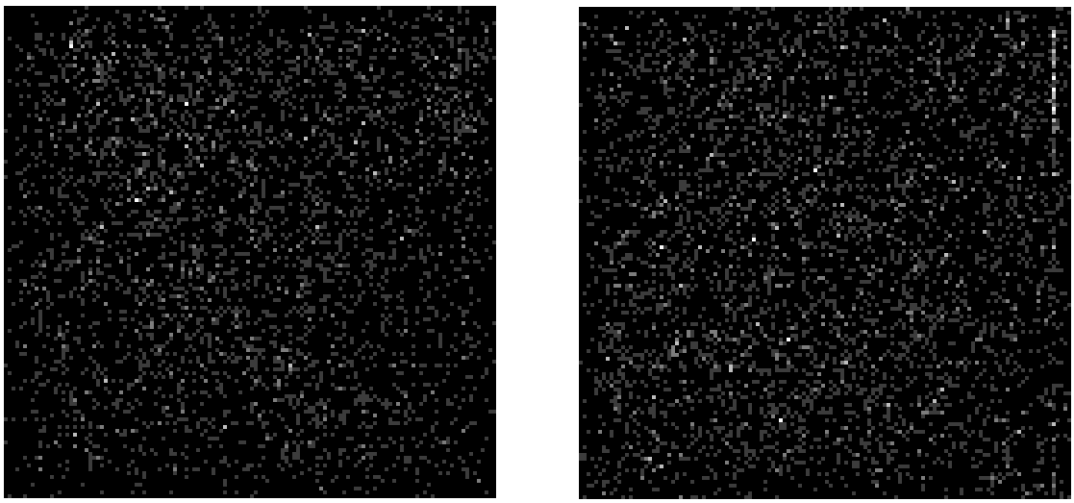

Figure 9: Density images of "lost" RTS pixels, e.g. no longer detected RTS on the dark ramps after irradiation (left) and of "new" RTS pixels, e.g. those not detected before irradiation (right) with a minimum amplitude threshold of 35e-. Clearly the events seem randomly distributed and especially no spatial correlation to the irradiation beam footprint can be seen on the right image. The right image nevertheless shows some effect of noise pick-up (upper right corner), which leads to false spike-like, high frequency RTS detections.

3.3 Temperature

For the long dark UTR acquisition three different SCA operating temperatures were used: 80K, 85K and 90K. The impact of temperature on amplitude and period was investigated for the RTS pixels detected at all three temperatures. All analysed SCAs showed the same behaviour as shown in Figure 10. The RTS amplitude is preserved while the RTS period on average gets shorter (higher frequency) for higher temperature by a factor of approximately 2 for each 5 degrees Celsius temperature change. As a consequence, the RTS population at higher temperature is also characterised by the strong reduction in long period (low frequency) RTS as can be seen from Figure 11.

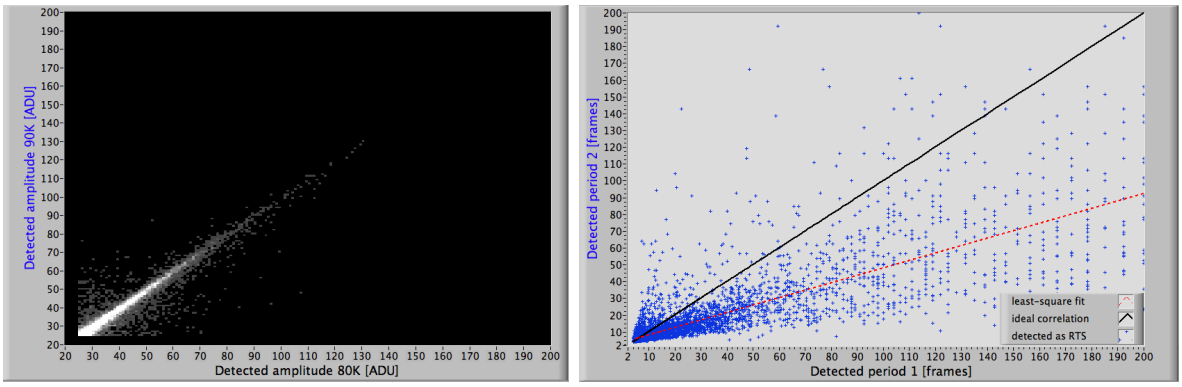

Figure 10: (Left) density plot of detected amplitude for the same RTS pixels on ramps for 80K vs. 90K. Most amplitude pairs scatter around the identical relation, therefore the amplitude seems preserved under temperature changes. (Right) Scatter plot of detected period for the same RTS pixels on ramps for 80K vs. 85K. For higher temperature the period seems shorter, e.g. to move to higher frequency.

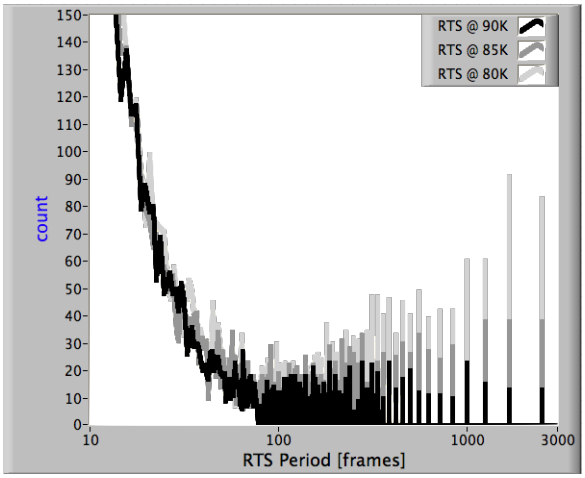

Figure 11: Histogram of RTS periods for one analysed SCA and the RTS pixels detected on all three operating temperature UTR (80K, 85K sand 90K). All SCAs show the same behaviour of reduction in number of long period (low frequency) RTS pixels towards higher operating temperature.

3.4 Geometrical

During the initial study some geometrical inhomogeneity was hinted related to the so-called “picture frame” effect in the baseline image. All analysed SCAs showed this picture frame baseline image, and there is a clear correlation to the distribution of detected RTS as can be seen on Figure 12. Otherwise the geometrical distribution is fairly homogeneous. To avoid any problems with spurious noise pick-up, a RTS detection threshold of at least 50e- amplitude was used. Glitches caused by cosmic rays were filtered out as well.

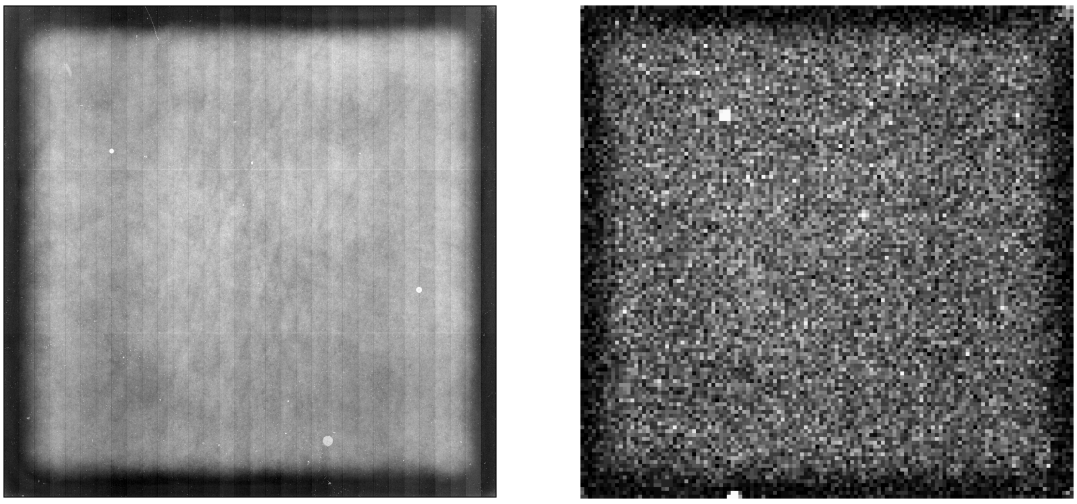

Figure 12: (Left) Average baseline (pedestal) image constructed by averaging over the first frame from all analysed dark UTR at 90K of the 16 Flight SCAs. The "picture frame" caused by lower baseline values on the outer detector image area is clearly seen. (Right) Average density image of detected RTS on the 16 Flight SCAs at 90K. Apart from local concentrations on some SCAs the distribution of RTS over the image area is homogeneous with the exception of a lower density corresponding to the picture frame area.

4. FLIGHT SCA STATISTICS

Table 3: Detected RTS pixels statistics at 90K for all Flight SCAs

SCA	Image area pixels, all RTS candidates (total and [%])	Image area pixels, amplitude ≥ 50e- (total and [%])	Image area pixels, amplitude ≥ 100e- (total and [%])	Reference pixels, all RTS candidates (total and [%])	Reference pixels, amplitude ≥ 50e- (total and [%])	Reference pixels, amplitude ≥ 100e- (total)
1	34712 (0.83%)	7855 (0.19%)	1814 (0.04%)	103 (0.31%)	15 (0.05%)	1
2	13616 (0.33%)	5353 (0.13%)	890 (0.02%)	98 (0.30%)	19 (0.06%)	0
3	28817 (0.69%)	13037 (0.31%)	2183 (0.05%)	156 (0.48%)	21 (0.06%)	0
4	25499 (0.61%)	12023 (0.29%)	2051 (0.05%)	121 (0.37%)	16 (0.05%)	1
5	14738 (0.35%)	6803 (0.16%)	1016 (0.02%)	149 (0.46%)	31 (0.10%)	0
6	16017 (0.38%)	7838 (0.19%)	1190 (0.03%)	121 (0.37%)	20 (0.06%)	1
7	16877 (0.41%)	7928 (0.19%)	1404 (0.03%)	94 (0.29%)	22 (0.07%)	0
8	47024 (1.13%)	5976 (0.14%)	1058 (0.03%)	117 (0.36%)	12 (0.04%)	0
9	35278 (0.85%)	9622 (0.23%)	1844 (0.04%)	161 (0.49%)	19 (0.06%)	0
10	14316 (0.34%)	7733 (0.19%)	1306 (0.03%)	96 (0.29%)	15 (0.05%)	0
11	15355 (0.37%)	9410 (0.23%)	2165 (0.05%)	73 (0.22%)	16 (0.05%)	0
12	36584 (0.88%)	8220 (0.20%)	1577 (0.04%)	137 (0.41%)	21 (0.06%)	1
13*	15860 (0.38%)	7656 (0.18%)	1816 (0.04%)	202 (0.62%)	29 (0.09%)	0
14*	41153 (0.99%)	16600 (0.40%)	4596 (0.11%)	160 (0.49%)	43 (0.12%)	1
15	38149 (0.92%)	6163 (0.15%)	1257 (0.03%)	100 (0.31%)	25 (0.08%)	1
16*	23500 (0.56%)	10027 (0.24%)	1643 (0.04%)	123 (0.38%)	28 (0.08%)	2
Average	**26093 (0.63%)**	**8890 (0.21%)**	**1738 (0.04%)**	**126 (0.38%)**	**22 (0.07%)**	**0.5 (0.002%)**

* Reduced UTR of 4000 frames used (see explanation in text)

A statistical analysis of RTS pixels has been carried out on all Flight SCAs. Different amplitude thresholds have been set and image area and reference pixels analysed separately. Number counts vary between the SCAs but at higher amplitude thresholds stay within a factor of 2.

In the case of no amplitude threshold filtering (only inherent algorithm efficiency), SCA13 and SCA14, and to a lesser extend also SCA16, showed a strong deviation of low-amplitude RTS to high counts. In case of SCA13 and SCA16 the higher amplitude threshold counts are in line with the other SCAs, while SCA14 consistently shows higher number counts. Non-linear background was suspected, and indeed limiting the analysis to the last 4000 CDS frames (with the caveat of a slightly reduced algorithm efficiency) brought the numbers back in line with the other SCAs and which is reported in Table 3. With this amendment, the detected RTS populations stay on average at 0.6% of all image area pixels and 0.4% of all reference pixels. Both is below the 1% from expected from the original study and showing a slight imbalance between image area and reference pixels.

5. CONCLUSIONS

Several possible dependencies of RTS population and RTS parameter values have been analysed in more detail with respect to the initial RTS study. Data from all Euclid Flight SCAs has been used together with data from specific tests on engineering grade devices. Still some further investigations of unexpected results and to disentangle environmental effects are pending. Among the studied dependencies the following conclusions can be drawn:

- **Thermal cycling**: this seems to have an impact on the overall RTS population with newly created RTS and disappearing RTS. How much of this might be attributed to long ambient temperature storage is still pending.
- **Proton irradiation**: this seems to have no impact on RTS; most of the changes to RTS population seem to be related to thermal cycling and long duration ambient temperature exposure (or annealing) rather than proper radiation damage.
- **Temperature**: the expected effect of increasing frequency of RTS transitions with increasing temperature in line with the theory of trapping/de-trapping as the origin of RTS has been confirmed.
- **Geometrical**: the suspected correlation of RTS pixel density with the "picture frame" baseline non-uniformity has been confirmed. This seems to point to a material stress related origin of appearance of RTS in the image area pixels.
- **Overall statistics**: from the original study the expected amount of RTS pixels with respect to the overall number of pixels in the image and reference pixel areas, respectively, was about 1% (within the remit of algorithm performance). This seems to be slightly overestimated: the average numbers from the 16 Flight SCAs rather point to about 0.6% for the image area pixels and about 0.4% for the reference pixels.

REFERENCES

[1] Kohley, R., et al., "Random telegraph signal (RTS) noise and other anomalies in the near-infrared detector systems for the Euclid mission", Proc. SPIE 9915, (2016)
[2] Racca, G., et al., "The Euclid mission design", Proc. SPIE 9904, (2016)
[3] Maciaszek, T., "Euclid near infrared spectrometer and photometer instrument description frozen at the critical design review", Proc. SPIE 10698, (2018)
[4] Bai, Y., et al., "Manufacturability and performance of 2.3-μm HgCdTe H2RG sensor chip assemblies for Euclid", Proc. SPIE 10709, (2018).
[5] Secroun, A., et al., "Flight H2RG IR detectors: on-ground characterization for the Euclid NISP instrument", Proc. SPIE 10709, (2018).
[6] Barbier, R., et al., "Detector chain calibration strategy for the Euclid flight IR H2RGs", Proc. SPIE 10709, (2018).
[7] Crouzet, P., et al., "Euclid H2RG detectors: Impact of crosshatch patterns on photometric and centroid errors and persistence mitigation tests", Proc. SPIE 10709, (2018).